Time-Optimal Parameterization of Geometric Paths for Fixed-Wing Aircraft

Yiming Zhao* and Panagiotis Tsiotras†

School of Aerospace Engineering, Georgia Institute of Technology, Atlanta, GA, 30332-0150

We propose a method for minimum-time travel along a prescribed geometric path for a fixed-wing aircraft subject to given state and control constraints. The method checks the feasibility of the path, namely, whether it is possible for the aircraft to travel along the path without violating any of the state or control constraints. If the path is feasible, the method subsequently finds a semi-analytical solution of the velocity profile to minimize the time of travel along the given path, while satisfying the prescribed control bounds. The optimal speed profile is used to time-parameterize the path, and subsequently generate the state and control histories via inverse dynamics. Two algorithms for generating the optimal velocity profile are proposed and are compared with existing time-optimal control algorithms. Numerical examples are presented to show the validity, numerical accuracy and optimality of the proposed method.

I. Introduction

Several path-planning methods such as A^*, D^*, concatenations of Dubins' path primitives, potential field methods, etc, exist in the literature.[1–4] These have become very popular owing to their numerical efficiency and optimality. These methods typically work on a subset of the state space and, in general, may not provide information about the control histories required for maneuvering the aircraft to follow the optimal path. In practice, the implementation of these path-planning methods requires trajectory tracking controllers (or human pilots) in order to generate the required control commands. Because most of these path-planning methods are at the kinematic level and do not account for the dynamics of the aircraft, the feasibility of the path is not guaranteed a priori, i.e., it is possible that no control exists that allows the aircraft to follow the proposed path without violating the control or state constraints.

An alternative approach to flight path-planning, which considers more realistic dynamics of the aircraft and incorporates the state/control constraints, formulates flight-path planning as an optimal control problem. For the numerical solution of optimal control problems, the convergence and speed of the solution depends heavily on the initial guess of the time histories of both the state and control variables. A good initial guess can help the solution converge much faster. For a flight path-planning problem, while it is possible to figure out a reasonable initial guess for (part of) the state variables, the control histories that are consistent with this initial guess may be difficult to obtain.

The problem of optimal aircraft velocity profile generation is somewhat similar to the time-optimal control of robotic manipulators[5–9]. These approaches take advantage of the Lagrangian form of the dynamics, and give the minimum time speed profile for robotic manipulators to move along a specified path in minimum time. In this paper, we take a similar approach, and time-parameterize a given geometric path for a fixed-wing aircraft in a way that provides minimum-time optimality, while satisfying the dynamic and control constraints (if this is possible) for the given path. The proposed method works suitably well as a post-processing tool for pure geometric/kinematic planners to check feasibility of the generated path and for constructing good initial guesses for trajectory optimization solvers. Specifically, the method can be used as a bridge between the geometric path-planning methods and NLP approaches for solving optimal control problems.[10–13] The geometric path given by the former can be optimally time-parameterized to obtain the corresponding state and control histories, which can then be passed to the NLP solver as an initial guess.

*Ph.D. candidate, AIAA student member, Email: yzhao7@gatech.edu.

†Professor, AIAA Fellow, Email: tsiotras@gatech.edu.

In the rest of the paper we first show that the problem of optimal time-parameterization of a geometric path for a fixed-wing aircraft can be converted to a constrained *scalar* functional optimization problem by decoupling the controls. The analytical solution to this problem is derived using Pontryagin's Maximum Principle. The switching structure of the optimal control is studied, and the concept of the admissible speed set is introduced for searching the optimal speed profile given an arbitrary path. Two algorithms are proposed, which achieve superior numerical efficiency compared with other similar algorithms. Numerical examples dealing with the time-parameterization of a Dubins-like path, and a minimum-time travel path, respectively, for minimum-time to land of a civilian aircraft are presented to demonstrate the proposed method.

II. Aircraft Model

Geometric path-planning methods generate planar or three-dimensional paths, and do not take into account the dynamics of the problem. Hence, they do not provide the trajectory (i.e., the time-parameterized path) in the ambient space. In other words, the coordinates x, y, z defining the path are not functions of time, t, but are rather expressed using the path coordinate, s, as follows: $x = x(s)$, $y = y(s)$, $z = z(s)$, where $s \in [s_0, s_f]$. The main objective of this work is to find a time-parameterization along s, i.e., a function $s(t)$, where $t \in [0, t_f]$ such that the corresponding time-parameterized trajectory $(x(s(t)), y(s(t)), z(s(t)))$ satisfies a certain objective, for example, it minimizes t_f. Similarly to Ref. [6], we will assume that $x(s)$, $y(s)$, $z(s)$ are C^1 and piecewise analytic with respect to s. Specifically, the C^1 assumption guarantees the continuity of the speed, while the piecewise analytic assumption ensures certain smoothness such that the time optimal control algorithm terminates in a finite number of steps, as shown in [6]. Both assumptions can be satisfied by current path planning algorithms.

Consider the following equations of motion for a point-mass model of a fixed-wing aircraft:[14]

$$\dot{x} = v\cos\gamma\cos\psi, \tag{1}$$

$$\dot{y} = v\cos\gamma\sin\psi, \tag{2}$$

$$\dot{z} = v\sin\gamma, \tag{3}$$

$$\dot{v} = \frac{1}{m}\left[T - D(C_L, v, \rho) - mg\sin\gamma\right], \tag{4}$$

$$\dot{\gamma} = \frac{1}{mv}\left[L(C_L, v, \rho)\cos\phi - mg\cos\gamma\right], \tag{5}$$

$$\dot{\psi} = -\frac{L(C_L, v, \rho)\sin\phi}{mv\cos\gamma}, \tag{6}$$

where x, y, z are the coordinates defining the position of the aircraft, v is its speed, ρ is the air density (varying with altitude), γ is the flight path angle, ψ is the heading angle, and ϕ is the bank angle. The aerodynamic lift force $L(C_L, v, \rho)$ and drag force $D(C_L, v, \rho)$ are given by:

$$L\left(C_L, v, \rho\right) = \frac{1}{2}\rho v^2 S C_L,$$

$$D\left(C_L, v, \rho\right) = \frac{1}{2}\rho v^2 S C_D = \frac{1}{2}\rho v^2 S (C_{D_0} + K C_L^2),$$

where C_{D_0} and K are constants determined by the aerodynamic properties of the aircraft, and S is the main wing surface area. In this model the lift coefficient C_L, the bank angle ϕ, and the thrust T are the control inputs. The effect of wind is not considered.

Because the given path is naturally parameterized using the path coordinate s instead of time, the equations of motion can be rewritten with respect to s as follows (where prime denotes differentiation with

respect to s):

$$
\begin{aligned}
x' &= \cos\gamma\cos\psi, && (7)\\
y' &= \cos\gamma\sin\psi, && (8)\\
z' &= \sin\gamma, && (9)\\
v' &= \frac{1}{mv}\left[T - D\left(C_L, v\right) - mg\sin\gamma\right], && (10)\\
\gamma' &= \frac{1}{mv^2}\left[L\left(C_L, v\right)\cos\phi - mg\cos\gamma\right], && (11)\\
\psi' &= -\frac{L\left(C_L, v\right)\sin\phi}{mv^2\cos\gamma}. && (12)
\end{aligned}
$$

When deriving (7)-(12), the following relations have been used:

$$
\begin{aligned}
\mathrm{d}t &= \frac{\mathrm{d}s}{v}, && (13)\\
\mathrm{d}s &= \sqrt{\mathrm{d}^2x + \mathrm{d}^2y + \mathrm{d}^2z}, && (14)\\
\psi &= \arctan\frac{\mathrm{d}y}{\mathrm{d}x} = \arctan\frac{y'}{x'}, && (15)\\
\gamma &= \arctan\frac{\mathrm{d}z}{\sqrt{\mathrm{d}x^2 + \mathrm{d}y^2}} = \arctan\frac{z'}{\sqrt{x'^2 + y'^2}}, && (16)\\
\psi' &= \frac{1}{1 + (y'/x')^2}\frac{y''x' - y'x''}{x'^2} = \frac{x'^2}{x'^2 + y'^2}\frac{y''x' - y'x''}{x'^2} = \frac{y''x' - y'x''}{x'^2 + y'^2}, && (17)\\
\gamma' &= \frac{z''x'^2 + z''y'^2 - z'x''x' - z'y''y'}{\sqrt{x'^2 + y'^2}}. && (18)
\end{aligned}
$$

Note that the flight path angle γ and the heading angle ψ are purely geometric variables. Once a three-dimensional path $(x(s), y(s), z(s))$ is given, these variables and their derivatives with respect to the path coordinate can be easily computed. It is clear that the C^1 and piecewise analyticity of the path implies the piecewise analyticity of all states and their derivatives. The time histories of the state and control variables are usually not uniquely determined from $(x(s), y(s), z(s))$. Indeed, there may be many ways to fly along a given path—for instance, the aircraft has the option to fly faster or slower along certain parts of the path.

In order to time-parameterize an arbitrary path, it is sufficient to obtain the history of the speed $v(s)$ with respect to the path coordinate s. If the optimal speed profile $v^*(s)$ is obtained, the corresponding optimal time-parameterization of the trajectory can be calculated by integrating (13). Specifically, let $t^* : [s_0, s_f] \to [0, t_f]$ be the bijective mapping between the path coordinate and the corresponding time coordinate along the optimal solution. Then $t^*(s)$ denotes the time at which the aircraft arrives at the position corresponding to path coordinate s. Since $\mathrm{d}t^* = \mathrm{d}s/v^*(s)$, it follows that the optimal time profile along the path is given by

$$
t^*(s) = \int_{s_0}^{s} \mathrm{d}t^* = \int_{s_0}^{s} 1/v^*(s)\mathrm{d}s, \qquad s_0 \le s \le s_f.
$$

The optimal time-parameterization of the geometric trajectory $\big(x(s), y(s), z(s)\big)$ is then given by

$$
\big(x^*(t), y^*(t), z^*(t)\big) = \big(x(t^{*-1}(t)), y(t^{*-1}(t)), z(t^{*-1}(t))\big).
$$

It will be shown in Section V that the optimal thrust profile $T^*(s)$ along the path can be determined once $v^*(s)$ is known. Subsequently, the other controls can be recovered though inverse dynamics as follows:

$$
\begin{aligned}
C_L^*(s) &= \frac{2}{\rho v^{*2}(s) S}\left(T^*(s) - mv^*(s)v^{*\prime}(s) - mg\sin\gamma(s)\right),\\
\phi^*(s) &= -\arctan\left(\frac{\cos\gamma(s)\psi'(s)}{\gamma'(s) + g\cos\gamma(s)/v^{*2}(s)}\right).
\end{aligned}
$$

Hence, the key to the optimal time-parameterization of a geometric path is the optimization of the speed profile along the given path. Next, we characterize two algebraic constraints and one differential constraint, which will be used in the sequel to find the optimal speed profile.

III. Control Constraints

We assume that the lift coefficient C_L, the bank angle ϕ, and the thrust T must stay within certain ranges, namely,

$$C_L(s) \in [C_{L_{\min}}(s),\, C_{L_{\max}}(s)], \quad \phi(s) \in [\phi_{\min}(s), \phi_{\max}(s)], \quad T(s) \in [T_{\min}(s), T_{\max}(s)], \quad \forall s \in [s_0, s_f], \quad (19)$$

where $C_{L_{\min}}$, $C_{L_{\max}}$, $\phi_{\min}$, $\phi_{\max}$, $T_{\min}$ and $T_{\max}$ are piecewise analytic functions of s. We also assume that the aircraft speed satisfies the bound $v(s) \in [v_{\min}(s), v_{\max}(s)]$, where $v_{\min}$ and $v_{\max}$ are piecewise analytic functions with $v_{\min}(s) > 0$ for all $s \in [s_0, s_f]$. These constraints account for limitations of the control inputs which depend on the location along the path. For example, the engine power generally varies with respect to the altitude. Furthermore, during the touch-down and take-off phases, the aircraft's bank angle must be almost zero, and gear and lift-generation devices such as flaps are also employed, which change the lift-drag coefficients of the aircraft. We will further assume that $C_{L_{\min}}(s) \leq 0 \leq C_{L_{\max}}(s)$, $-\pi/2 < \phi_{\min}(s) \leq 0 \leq \phi_{\max}(s) < \pi/2$, and $0 \leq T_{\min}(s) \leq T_{\max}(s)$, for all $s \in [s_0, s_f]$. It is also assumed that the flight path angle satisfies $\gamma(s) \in (-\pi/2, \pi/2)$. These are generic conditions for a civil aircraft in normal/maneuverable flight conditions. When the aircraft is flying at an abnormal condition (due to malfunction of the control surfaces/servo systems/engines, structure-damage, etc.), these assumptions may no longer hold. Nonetheless, the method we introduce in this paper can still be applied with minor modifications. In such cases, the bounds on C_L, ϕ and T in (19) have to be updated to account for the post-failure characteristics of the airplane.

For notational convenience, henceforth $\Omega \triangleq v^2$ will be used to describe the constraints on the speed v. Since v is always positive, there is an one-to-one correspondence between v and Ω, and this replacement of the variable v with Ω does not change the original problem. Henceforth, Ω will be referred to as the 'speed-square' of the aircraft.

III.A. Lift Coefficient Constraint

From equations (11) and (12), we have

$$\gamma' = \frac{1}{2m}\rho S C_L \cos\phi - \frac{g\cos\gamma}{v^2}, \quad (20)$$

$$\psi' = -\frac{\rho v^2 S C_L \sin\phi}{2mv^2\cos\gamma} = -\frac{\rho S C_L \sin\phi}{2m\cos\gamma}, \quad (21)$$

which can be rewritten as:

$$C_L\cos\phi = \frac{2m}{\rho S}\left(\gamma' + \frac{g\cos\gamma}{v^2}\right), \quad (22)$$

$$C_L\sin\phi = -\frac{2m\psi'\cos\gamma}{\rho S}. \quad (23)$$

Eliminating ϕ from equation (22) and (23), and replacing v^2 with Ω, one obtains

$$\Omega = g_1(C_L;\gamma,\gamma',\psi') \triangleq \frac{2mg\cos\gamma}{\rho S}\left(\sqrt{C_L^2 - \left(\frac{2m\psi'\cos\gamma}{\rho S}\right)^2} - \frac{2m\gamma'}{\rho S}\right)^{-1}. \quad (24)$$

The other solution is omitted because it is always negative. Let

$$g_{1d}(C_L;s) \triangleq \sqrt{C_L^2(s) - \left(\frac{2m\psi'(s)\cos\gamma(s)}{\rho(s)S}\right)^2} - \frac{2m\gamma'(s)}{\rho(s)S}.$$

Then the well-posedness and positivity of Ω requires the existence of C_L such that $C_L \in [C_{L_{\min}}(s),\, C_{L_{\max}}(s)]$ and $g_{1d}(C_L;s) > 0$ for all $s \in [s_0, s_f]$, which is equivalent to the condition

$$\bar{C}_L(s) > \tilde{C}_L(s), \qquad \forall s \in [s_0, s_f], \quad (25)$$

where

$$\bar{C}_L(s) = \max\{-C_{L_{\min}}(s), C_{L_{\max}}(s)\}, \tag{26}$$

and

$$\tilde{C}_L(s) = \begin{cases} \dfrac{2m}{\rho(s)S}\,|\psi'(s)|\cos\gamma(s), & \text{if } \gamma'(s) < 0, \\ \dfrac{2m}{\rho(s)S}\sqrt{\gamma'^2(s) + \psi'^2(s)\cos^2\gamma(s)}, & \text{if } \gamma'(s) \geq 0. \end{cases} \tag{27}$$

Hence the given path is feasible when $\bar{C}_L(s) > \tilde{C}_L(s)$ for all $s \in [s_0, s_f]$; otherwise the path cannot be followed due to insufficient lift.

Assuming that the given path is feasible, condition (25) implies that $g_{1d}(C_L; s)$ is positive for all $s \in [s_0, s_f]$. Because equation (24) is a monotonically decreasing function with respect to C_L^2, the limit on the lift coefficient imposes a lower bound on the admissible speed-square Ω as follows:

$$\Omega(s) \geq \underline{g}_{w1}(s) \triangleq g_1(\bar{C}_L; \gamma, \gamma', \psi'). \tag{28}$$

Notice that $\underline{g}_{w1}(s)$ is differentiable with respect to s due to the feasibility assumption.

III.B. Bank Angle Constraint

When $C_L(s) = 0$ for some $s \in [s_0, s_f]$, the lift is zero, and the bank angle ϕ is not determined at that instant. In this case, the bounds of the bank angle ϕ do not constrain the admissible speed Ω at s. Similarly, if $\gamma'(s) + g\cos\gamma(s)/\Omega(s) = 0$, $\gamma'(s) \neq 0$ since $g\cos\gamma(s)/\Omega(s) > 0$, and $\Omega(s)$ is uniquely determined regardless of the choice of ϕ. Therefore, assuming that $C_L \neq 0$, $\gamma'(s) + g\cos\gamma(s)/\Omega(s) \neq 0$, and eliminating C_L from equations (22) and (23), we have

$$\tan\phi = -\frac{\psi'\cos\gamma}{\gamma' + g\cos\gamma/\Omega}. \tag{29}$$

Solving for Ω from equation (29) yields:

$$\Omega = g_2(\phi; \gamma, \gamma', \psi') \triangleq -\frac{g\cos\gamma\tan\phi}{\gamma'\tan\phi + \psi'\cos\gamma}. \tag{30}$$

The positivity of $\Omega(s)$ requires that $g_2(\phi(s); \gamma(s), \gamma'(s), \psi'(s)) > 0$ for all $s \in [s_0, s_f]$, otherwise the path is infeasible. Assuming therefore that $g_2(\phi; \gamma, \gamma', \psi') > 0$, the constraints on Ω due to the bank angle bounds can be determined as follows:

(i) When $\psi'(s) = 0$, equation (29) implies that $\phi(s) = 0$, and the bounds of ϕ impose no constraint on $\Omega(s)$.

(ii) When $\psi'(s) \neq 0$, two cases need to be considered:

(iia) If $\gamma'(s) = 0$, since $\gamma \in (-\pi/2, \pi/2)$, we have

$$\Omega(s) = g_2(\phi(s); \gamma(s), \gamma'(s), \psi'(s)) = -\frac{g\tan\phi(s)}{\psi'(s)}$$

The assumption $g_2(\phi(s); \gamma(s), \gamma'(s), \psi'(s)) > 0$ requires that $\phi(s)\psi'(s) < 0$. Then the constraint on ϕ imposes the following upper bound on the speed-square Ω

$$\Omega(s) \leq \overline{g}_{w1}(s) \triangleq \begin{cases} \max\{\dfrac{g\tan\phi_{\min}}{\psi'(s)}, \dfrac{g\tan\phi_{\max}}{\psi'(s)}\}, & \gamma'(s) = 0 \text{ and } \psi'(s) \neq 0 \\ v_{\max}^2(s), & \text{otherwise.} \end{cases} \tag{31}$$

(iib) If $\gamma'(s) \neq 0$, rewrite (30) as follows:

$$\gamma'(s)\tan\phi(s) + \psi'(s)\cos\gamma(s) = -\frac{g\cos\gamma(s)}{\Omega(s)}\tan\phi(s) \tag{32}$$

Equation (32) limits the admissible values of $\Omega(s)$ such that $\phi(s) \in [\phi_{\min}(s), \phi_{\max}(s)]$. A necessary and sufficient condition for this is

$$\frac{g\cos\gamma(s)}{\Omega(s)} \leq \min\left\{-h(\phi_{\min};\gamma,\gamma',\psi'), -h(\phi_{\max};\gamma,\gamma',\psi')\right\}, \tag{33}$$

or

$$\frac{g\cos\gamma(s)}{\Omega(s)} \geq \max\left\{-h(\phi_{\min};\gamma,\gamma',\psi'), -h(\phi_{\max};\gamma,\gamma',\psi')\right\}, \tag{34}$$

where

$$h(\phi;\gamma,\gamma',\psi') \stackrel{\triangle}{=} \gamma' + \psi'\cos\gamma/\tan\phi. \tag{35}$$

In order to characterize the constraint on Ω induced by the bank angle constraint, three subcases need to be considered:

(iib.1) If $\max\{-h(\phi_{\min};\gamma,\gamma',\psi'), -h(\phi_{\max};\gamma,\gamma',\psi')\} \leq 0$, the bank angle constraint does not impose any constraint on $\Omega(s)$;

(iib.2) If $\min\{-h(\phi_{\min};\gamma,\gamma',\psi'), -h(\phi_{\max};\gamma,\gamma',\psi')\} \leq 0$, this is a test $\max\{-h(\phi_{\min};\gamma,\gamma',\psi'), -h(\phi_{\max};\gamma,\gamma',\psi')\} > 0$, then the constraint on $\Omega(s)$ is given by

$$\Omega(s) \leq g\cos\gamma(s)\left(\max\left\{-h(\phi_{\min};\gamma,\gamma',\psi'), -h(\phi_{\max};\gamma,\gamma',\psi')\right\}\right)^{-1}. \tag{36}$$

(iib.3) Finally, if $\min\left\{-h(\phi_{\min};\gamma,\gamma',\psi'), -h(\phi_{\max};\gamma,\gamma',\psi')\right\} > 0$, then it is required that either (36) holds, or the following inequality holds:

$$\Omega(s) \geq g\cos\gamma(s)\left(\min\left\{-h(\phi_{\min};\gamma,\gamma',\psi'), -h(\phi_{\max};\gamma,\gamma',\psi')\right\}\right)^{-1}. \tag{37}$$

III.C. Thrust Constraint

From equations (10), (22) and (23) we have the following equation:

$$\begin{aligned} T &= mvv' + \left(\frac{1}{2}C_{D_0}\rho S + \frac{2Km^2\gamma'^2}{\rho S} + \frac{Km^2\cos^2\gamma\psi'^2}{\rho S}\right)v^2 \\ &\quad + \frac{2Km^2g^2\cos^2\gamma}{\rho S}\frac{1}{v^2} + \frac{4Km^2\gamma' g\cos\gamma}{\rho S} + mg\sin\gamma. \end{aligned}$$

Note that since $vv' = v\frac{\mathrm{d}v}{\mathrm{d}s} = \frac{1}{2}\frac{\mathrm{d}v^2}{\mathrm{d}s} = \frac{1}{2}\Omega'$, the above equation can be rewritten as a constraint on the derivative of Ω as follows

$$\Omega'(s) = \frac{2T(s)}{m} + c_1(s)\Omega(s) + c_2(s)\frac{1}{\Omega(s)} + c_3(s), \tag{38}$$

where

$$c_1(s) \stackrel{\triangle}{=} \frac{C_{D_0}(s)\rho(s)S}{m} + \frac{4Km\gamma'^2(s)}{\rho(s)S} + \frac{2Km\cos^2\gamma(s)\psi'^2(s)}{\rho(s)S}, \tag{39}$$

$$c_2(s) \stackrel{\triangle}{=} -\frac{4Kmg^2\cos^2\gamma(s)}{\rho(s)S}, \tag{40}$$

$$c_3(s) \stackrel{\triangle}{=} -\frac{8Km\gamma'(s)g\cos\gamma(s)}{\rho(s)S} - 2g\sin\gamma(s). \tag{41}$$

Note that c_1,c_2 and c_3 are piecewise analytic functions with respect to s.

IV. Intermediate Control and the Admissible Speed Set

We say that a control is intermediate when it is not bang-bang. In general, intermediate control arises when an algebraic constraint is active. The algebraic constraints may either be specified a priori, or come from differential constraints that reduce to algebraic constraints over part or all of the trajectory. For the case of robotic manipulators [5–9], only differential constraints exist, and intermediate control arcs arise when the inertia matrix becomes singular, with the corresponding differential constraint reduced into an algebraic constraint. For the case of fixed-wing aircraft, both (11) and (12) are algebraic, and intermediate controls are more frequently observed, as will be shown later in the paper.

In the previous section, control constraints (the lift coefficient constraint and the bank angle constraint) have been reduced to a series of algebraic constraints on the speed square Ω. The optimal speed profile must be found among all functions that satisfy both the algebraic constraints and the differential constraint (38). The concept of admissible acceleration range in the $\dot{s}^2 - \ddot{s}$ plane has been proposed for the time optimal control of robotic manipulators.[7,8] Due to the Lagrangian form of the dynamics, the admissible acceleration range in this case is a convex polygon at each point along the path, and the acceleration maximizing the speed corresponds to a certain vertex most of the time, but the required acceleration is not obvious when some controls are intermediate. In Ref. [6] the inadmissible region is defined as the set of points in the $s - \dot{s}^2$ plane where the differential constraints becomes incompatible, revealing more information about the topology of the set on which the optimization is carried out. However, as pointed out in Ref. [8], the assumption of maximum and minimum acceleration in Ref. [6] fails at intermediate control points and arcs, which may result in unbounded computation time and chattering controls.

For a better treatment of the different forms of constraints compared with existing methods, we first give a definition of compatibility for differential and algebraic constraints. To this end, consider a general time-optimal control problem involving differential constraints f_i, algebraic equality constraints g_j, and algebraic inequality constraints h_k as follows.

$$\Omega' = f_i\left(\Omega, u; s\right), \quad i = 1, 2, \ldots, N_f, \tag{42}$$

$$g_j\left(\Omega, u; s\right) = 0, \quad j = 1, 2, \ldots, N_g, \tag{43}$$

$$h_k\left(\Omega; s\right) \leq 0, \quad k = 1, 2, \ldots, N_h, \tag{44}$$

where $u(s) \in \mathcal{U}(s) \subseteq \mathbb{R}^m$ is the admissible control set at s. Since equation (43) determines implicitly a mapping from u to Ω, under mild assumptions we may assume that Eqn. (43) can be rewritten as $\Omega = \hat{g}_j(u; s)$. Then

The differential constraints f_i are compatible at (s, Ω) if $\bigcap_{i=1}^{N_f} f_i\left(\Omega, \mathcal{U}(s); s\right) \neq \emptyset$.

The algebraic equality constraints g_j are compatible at (s, Ω) if $\Omega \in \bigcap_{j=1}^{N_g} \hat{g}_j\left(\mathcal{U}(s); s\right)$.

The algebraic inequality constraints are compatible at (s, Ω) if $h_k\left(\Omega; s\right) \leq 0$ for all $k = 1, \ldots, N_{h,}$.

Definition IV.1. The admissible speed set $\mathcal{W}$ is a set in the $s - \Omega$ plane defined as the union of points where all differential and algebraic constraints (including the degenerate differential constraints) are compatible.

Let

$$\mathcal{W}_f = \left\{ (s, \Omega) | \bigcap_{i=1}^{N_f} f_i\big(\Omega, \mathcal{U}(s); s\big) \neq \emptyset, s \in \Big[s_0, s_f\Big] \right\} \tag{45}$$

$$\mathcal{W}_g = \left\{ (s, \Omega) | \, \Omega \in \bigcap_{j=1}^{N_g} \hat{g}_j\big(\mathcal{U}(s); s\big), s \in \Big[s_0, s_f\Big] \right\} \tag{46}$$

$$\mathcal{W}_h = \left\{ (s, \Omega) | \, h_k\left(\Omega; s\right) \leq 0, k = 1, \ldots, N_h, s \in \Big[s_0, s_f\Big] \right\} \tag{47}$$

so that $\mathcal{W} = \mathcal{W}_f \bigcap \mathcal{W}_g \bigcap \mathcal{W}_h$. We need to find within $\mathcal{W}$ a speed-square profile $\Omega(s)$ that minimizes the travel time. For the fixed-wing aircraft time-optimal control problem, equation (38) is the only differential

constraint, which is trivially compatible with itself everywhere in the $s-\Omega$ plane because $f(\Omega,\mathcal{U};s)\neq\emptyset$ for all $(s,\Omega)\in\mathbb{R}^2$, so $\mathcal{W}$ is determined only by the algebraic constraints. The boundary of $\mathcal{W}$ is generally difficult to characterize. However, for the dynamics of fixed-wing aircraft, the boundary of $\mathcal{W}$ can be described by piecewise analytic functions. The boundary of $\mathcal{W}$ for fixed-wing aircraft is determined by $v_{\min}$, $v_{\max}$ and the piecewise analytic functions in equations (28), (31), (36) and (37), which define the upper or lower bounds on $\Omega(s)$.

Let $\mathcal{W}_s \triangleq \{(s,\Omega)\in\mathcal{W}\}$, $s\in[s_0,s_f]$, be the vertical slice of $\mathcal{W}$ at s. If $\mathcal{W}_s$ is empty for some s, then the specified path is not feasible. Note that when $\min\{-h(\phi_{\min};\gamma,\gamma',\psi'),-h(\phi_{\max};\gamma,\gamma',\psi')\}>0$, which is the case considered in (iib.3) in Section III.III.B, $\mathcal{W}_s$ may be disconnected on some subinterval of $[s_0,s_f]$. As a result, $\mathcal{W}$ is not simply connected, that is, it may contain holes in its interior[a]. If this is the case for a given path, then $\mathcal{W}$ can be decomposed into a finite number of partially over-lapping subsets such that $\mathcal{W}=\bigcup\mathcal{W}_i$, and for each subset $\mathcal{W}_i$, $\mathcal{W}_{i_S}$ is simply connected for all $s\in[s_0,s_f]$, as is shown in Fig. 1. The optimization can be performed in each $\mathcal{W}_i$ independently for the optimal speed profile candidates within $\mathcal{W}_i$, and the optimal solution is chosen by a comparison among a finite number of candidates. Note that the existence and the shape of the holes are not known a priori. When a hole exists, if the upper "corridor" which by-passes the hole contains any speed profile satisfying the boundary conditions, then the optimal speed profile must stay above the hole for a point-wise maximization of the speed. However, it is also possible that the upper "corridor" does not contain any feasible speed profile due to the thrust constraint. If this is the case, the optimal speed profile must be searched in the lower corridor below the hole. The decomposition approach addresses this problem. Similar decomposition schemes can be designed for $\mathcal{W}_i$ with multiple holes. Without loss of generality, we may therefore assume that $\mathcal{W}$ is simply connected, and it is given by

$$\mathcal{W}=\{(s,\Omega)|\underline{g}_w(s)\leq\Omega\leq\overline{g}_w(s),\, s\in[s_0,s_f]\}, \tag{48}$$

where $\overline{g}_w$ and $\underline{g}_w$ are piece-wise analytic functions determined by the speed constraint, the lift coefficient constraint, and the bank angle constraint. The expressions of $\overline{g}_w$ and $\underline{g}_w$ can be obtained based on the analysis in Section III. If more than one upper constraints on Ω exist for some subinterval of $[s_0,s_f]$, then $\overline{g}_w$ is given by the minimum of these upper limits. Similarly, $\underline{g}_w$ is given by the maximum of the lower limits on Ω. It is clear that $\overline{g}_w$ and $\underline{g}_w$ are left differentiable.

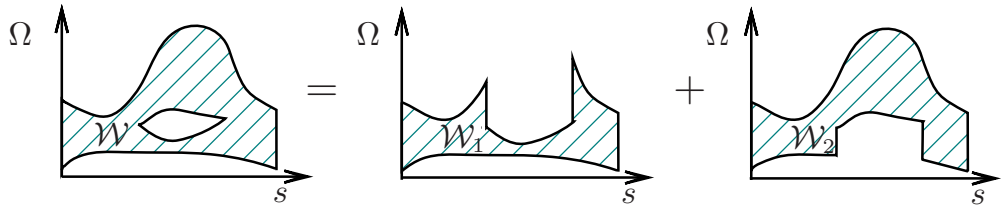

Figure 1. Decomposition of $\mathcal{W}$ when it is not simply connected.

V. Optimal Control Formulation

Instead of working with the original dynamical system described by (7) - (12), we now only need to solve an optimal control problem with a single state variable Ω and a single control input T. Let v_0 and v_f be the required initial and final speed at s_0 and s_f, respectively. We assume that $(s_0,v_0^2)\in\mathcal{W}_{s_0}$ and $(s_f,v_f^2)\in\mathcal{W}_{s_f}$.

It has been proved in Ref. [8] that (for the case of robotic manipulators) the control is bang-bang when the speed limit is not active. In this section we show a similar result for the thrust control of a fixed-wing aircraft. It is noted that although the bang-bang form of the control has been proved in Ref. [8], the switching structure between the upper and lower control bounds has not been studied, despite the fact that the appropriate structure has been used implicitly in the algorithms proposed in Ref. [5–9]. We therefore also prove in the sequel that for a fixed-wing aircraft, when the speed constraint is not active, the thrust control switching structure is unique.

[a]This is similar to the so-called "inadmissible island" in Ref. [6].

The optimal thrust profile T^* and the corresponding optimal speed $v^* = (\Omega^*)^{1/2}$ for the minimum-time travel of a fixed-wing aircraft are given by the solution to the following optimal control problem:

$$\begin{aligned}
\min_{T} \quad & J(s_0, s_f, \Omega(s_0), \Omega(s_f), T) = t_f = \int_{s_0}^{s_f} \frac{\mathrm{d}s}{\sqrt{\Omega}} \\
\text{subject to} \quad & \Omega'(s) = \frac{2T(s)}{m} + c_1(s)\Omega(s) + c_2(s)\frac{1}{\Omega(s)} + c_3(s), \\
& \Omega(s) \le \overline{g}_w(s), \\
& \Omega(s) \ge \underline{g}_w(s), \\
& \Omega(s_0) = v_0^2, \\
& \Omega(s_f) = v_f^2, \\
& T_{\min} \le T(s) \le T_{\max}.
\end{aligned} \tag{49}$$

The functions c_1, c_2 and c_3 are calculated as described in (39), (40) and (41), once the path is given. The Hamiltonian of the optimal control problem (49) is

$$\begin{aligned}
H(\Omega, \lambda, T, \overline{\mu}, \underline{\mu}, s) &= \frac{1}{\sqrt{\Omega}} + \lambda\left(\frac{2T}{m} + c_1\Omega + c_2\frac{1}{\Omega} + c_3\right) + \overline{\mu}(\Omega - \overline{g}_w) + \underline{\mu}(\underline{g}_w - \Omega) \\
&= \frac{2\lambda}{m}T + c_1\Omega\lambda + c_2\frac{1}{\Omega}\lambda + \frac{1}{\sqrt{\Omega}} + c_3\lambda + \Omega(\overline{\mu} - \underline{\mu}) - \overline{\mu}\,\overline{g}_w + \underline{\mu}\,\underline{g}_w
\end{aligned}$$

where $\overline{\mu}$ and $\underline{\mu}$ are the Kash-Kuhn-Tucker multipliers, satisfying the conditions

$$\begin{aligned}
&\overline{\mu} = 0 \text{ for } \Omega(s) < \overline{g}_w(s) \quad \text{and} \quad \overline{\mu} \ge 0 \text{ for } \Omega(s) = \overline{g}_w(s), \\
&\underline{\mu} = 0 \text{ for } \Omega(s) > \underline{g}_w(s) \quad \text{and} \quad \underline{\mu} \ge 0 \text{ for } \Omega(s) = \underline{g}_w(s).
\end{aligned}$$

The costate equation is

$$\lambda' = -\frac{\partial H}{\partial \Omega} = -c_1\lambda - c_2\lambda\frac{1}{\Omega^2} - \frac{1}{2}\Omega^{-2/3} + \overline{\mu} - \underline{\mu}. \tag{50}$$

The control T enters linearly into the Hamiltonian, so a singular control may exist. The switching function is

$$\frac{\partial H}{\partial T} = \frac{2\lambda}{m}.$$

Following Pontryagin's Maximum Principal, the optimal control T^* is given by

$$T^* = \underset{T \in [T_{\min}, T_{\max}]}{\arg\min} \; H(\Omega, \lambda, T, \overline{\mu}, \underline{\mu}, s) = \begin{cases} T_{\min}, & \text{for } \lambda > 0, \\ \text{singular control}, & \text{for } \lambda = 0, \\ T_{\max}, & \text{for } \lambda < 0. \end{cases}$$

Proposition V.1. No intermediate (singular) control exists when the speed limit constraints $\overline{g}_w$ and $\underline{g}_w$ are inactive.

Proof. We only need to show that when $\Omega < \overline{g}_w$ and $\Omega > \underline{g}_w$ there does not exist any sub-interval $[s_a, s_b] \subseteq [s_0, s_f]$ on which $\lambda(s) \equiv 0$. Suppose, ad absurdum, that $\lambda(s) \equiv \lambda'(s) \equiv 0$, for all $s \in [s_a, s_b]$. Because $\Omega < \overline{g}_w$ and $\Omega > \underline{g}_w$, $\overline{\mu} = \underline{\mu} = 0$ following the Kash-Kuhn-Tucker condition. Then on $[s_a, s_b]$, equation (50) becomes

$$0 = -\frac{1}{2}\Omega^{-2/3} < 0,$$

which is impossible. Hence λ cannot remain constantly zero on any nontrivial interval, and the proof is complete. □

Define the following operator which maps one positive piecewise analytic function into piecewise analytic function:

$$\Gamma(\cdot) \triangleq m\left(\partial_-(\cdot) - c_1(\cdot) - c_2\frac{1}{(\cdot)} - c_3\right), \tag{51}$$

where c_1, c_2 and c_2 are piecewise analytic functions given in equations (39) to (41). $\partial_-(\cdot)$ in (51) denotes the left derivative. Let $\overline{T}_w(s) \triangleq \Gamma \circ \overline{g}_w(s)$ and $\underline{T}_w(s) \triangleq \Gamma \circ \underline{g}_w(s)$. If $\Omega = \overline{g}_w$ on some subinterval $(s_a, s_b) \subseteq [s_0, s_f]$, namely, the upper speed limit is active for part of the optimal solution, then the corresponding thrust T is given uniquely by

$$T(s) = \overline{T}_w(s) \tag{52}$$

for all $s \in [s_a, s_b]$. Similarly, when $\Omega(s) = \underline{g}_w(s)$ over some non-empty sub-interval of $[s_0, s_f]$, we have that $T(s)$ is defined uniquely by $T(s) = \underline{T}_w(s)$.

Proposition V.2. Assume that the optimal thrust T^* exists on some subinterval $(s_a, s_b] \subseteq [s_0, s_f]$. If neither the upper nor the lower speed limit constraint is active for any $s \in (s_a, s_b]$, then T^* is bang-bang, and contains at most one switch, which is from $T_{\max}$ to $T_{\min}$.

Proof. Since we have shown that a singular control does not exist when the speed limit constraints are inactive, the control history must be bang-bang on $(s_a, s_b]$. We only need to prove that when the constraint is inactive there does not exist any switch from $T_{\min}$ to $T_{\max}$ in the optimal control T^*.

To this end, suppose, on the contrary, that T^* contains a switch from $T_{\min}$ to $T_{\max}$ at $s_m \in (s_a, s_b]$, such that

$$T^* = \begin{cases} T_{\min}, & s_a < s \le s_m, \\ T_{\max}, & s_m < s \le s_b. \end{cases}$$

Because $\Omega^*(s) - \overline{g}_w(s) < 0$ for all $s \in (s_a, s_b]$, there exists $\varepsilon > 0$ such that $\Omega^*(s) \le \overline{g}_w(s) - \varepsilon$ for all $s \in (s_a, s_b]$. Let $0 < \eta < \varepsilon$, and define the following trajectories passing through $(s_m, \Omega^*(s_m) + \eta)$

$$\Omega_m^-(s;\eta) = \Omega^*(s_m) + \eta + \int_{s_m}^{s} \left(\frac{T_{\min}}{m} + c_1(\tau)\Omega_m^-(\tau;\eta) + c_2(\tau)\frac{1}{v_m^-(\tau;\eta)} + c_3(\tau)\right) \mathrm{d}\tau$$

$$\Omega_m^+(s;\eta) = \Omega^*(s_m) + \eta + \int_{s_m}^{s} \left(\frac{T_{\max}}{m} + c_1(\tau)\Omega_m^+(\tau;\eta) + c_2(\tau)\frac{1}{v_m^+(\tau;\eta)} + c_3(\tau)\right) \mathrm{d}\tau$$

Note that Ω_m^- is a continuous function of s, hence $\Omega_m^{-\prime}(s;\eta)$ is continuous with respect to $T_{\min}$, η, and s. Similarly $\Omega_m^{+\prime}(s;\eta)$ is continuous with respect to $T_{\max}$, η, and s. Because $\Omega_m^{-\prime}(s_m;0) < \Omega^{*\prime}(s_m) < \Omega_m^{+\prime}(s_m;0)$, there exists positive real numbers η_1, and δ small enough such that $\Omega_m^{-\prime}(s;\eta) < \Omega^{*\prime}(s) < \Omega_m^{+\prime}(s;\eta)$ so long as $\eta < \eta_1$ and $s \in [s_m - \delta, s_m + \delta]$.

Let $\eta < \min\{\varepsilon, \eta_1\}$. Since $\Omega_m^{+\prime}(s;\eta) > \Omega^{*\prime}(s)$ for all $s \in [s_m - \delta, s_m + \delta]$ and $0 < \Omega_m^+(s_m;\eta) - \Omega^*(s_m) = \eta \le \varepsilon$, it is always possible to pick η_2 small enough such that $\Omega_m^+\left(s_m^-(\eta_2);\eta_2\right) = \Omega^*\left(s_m^-(\eta_2)\right)$ for some $s_m^-(\eta_2) \in [s_m - \delta, s_m)$. Then $\Omega_m^+(s;\eta_2) \le \Omega^*(s) + \varepsilon < \overline{g}_w(s)$ for all $s \in (s_m^+(\eta_2), s_m]$. Similarly, there exists $\eta_3 > 0$ such that $\Omega_m^-\left(s_m^+(\eta_3);\eta_3\right) = \Omega^*\left(s_m^+(\eta_3)\right)$ for some $s_m^+(\eta_3) \in (s_m, s_m + \delta]$, and $\Omega_m^+(s;\eta_2) < \overline{g}_w(s)$ for all $s \in (s_m, s_m^+(\eta_3)]$. Let $\eta < \min\{\varepsilon, \eta_1, \eta_2, \eta_3\}$, $s_m^- \triangleq s_m^-(\eta)$ and $s_m^+ \triangleq s_m^+(\eta)$.

Now consider a variation of T^* given by

$$\delta T = \begin{cases} T_{\max} - T_{\min}, & s_m^- < s \le s_m, \\ T_{\min} - T_{\min}, & s_m < s \le s_m^+, \\ 0, & \text{otherwise.} \end{cases}$$

The perturbed control $\widetilde{T} = T^* + \delta T$, is shown in Fig. 2. Let $\widetilde{\Omega}$ denote the corresponding speed profile, which is given by

$$\widetilde{\Omega}(s) = \Omega^*(s_a) + \int_{s_a}^{s} \left(\frac{\widetilde{T}}{m} + c_1(\tau)\widetilde{\Omega}(\tau) + c_2(\tau)\frac{1}{\widetilde{\Omega}(\tau)} + c_3(\tau) \right) \mathrm{d}\tau.$$

The variation of speed is shown in Fig. 3. By construction of δT it is clear that $\widetilde{\Omega} < \overline{g}_w$, $\Omega^*(s) = \widetilde{\Omega}(s)$ for $s \in (s_a, s_m^-]$ or $s \in [s_m^+, s_b]$, and $\Omega^*(s) < \widetilde{\Omega}(s)$ for $s \in (s_m^-, s_m^+)$. Hence $J(s_a, s_b, \Omega(s_a), \Omega(s_b), T^*) > J(s_a, s_b, \Omega(s_a), \Omega(s_b), \widetilde{T})$, and T^* cannot be optimal. □

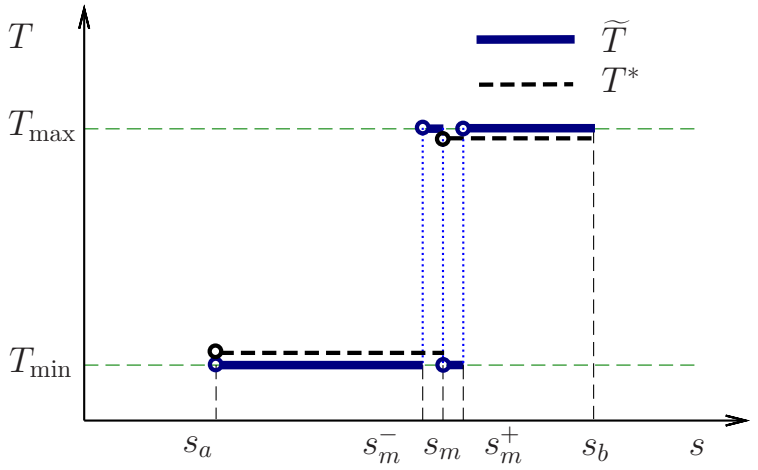

Figure 2. Thrust variation

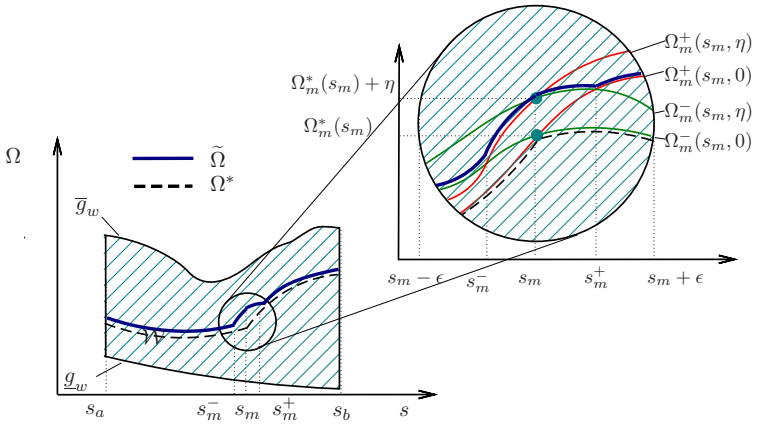

Figure 3. Speed variation

Proposition V.2 leads to the following lemma, which is important for the design of efficient algorithms for searching the time-optimal control along specified paths.

Lemma V.1. Assume that the optimal thrust T^* exists on some interval $[s_a, s_b] \subseteq [s_0, s_f]$. If the initial and final speed condition $\Omega(s_a) = \Omega_a$ and $\Omega(s_b) = \Omega_b$ cannot be satisfied with $T^* = T_{\max}$, or $T^* = T_{\min}$, or with T^* being a combination of $T_{\max}$ and $T_{\min}$ containing one switch, then $\Omega^* = \overline{g}_w$ on some subset of $[s_a, s_b]$.

The next proposition shows that $\underline{g}_w$ cannot be part of the optimal speed profile.

Proposition V.3. Assume that $\overline{g}_w \neq \underline{g}_w$, and $T_{\min} \leq \underline{T}_w < T_{\max}$ on some subinterval (s_a, s_b), then $\Omega^*(s) \neq \underline{g}_w(s)$ for all $s \in (s_a, s_a)$.

Proof. If $\Omega^*(s) = \underline{g}_w(s)$ for some $s \in (s_a, s_b) \subset [s_0, s_f]$, then since $\overline{g}_w \neq \underline{g}_w$ and $T_{\min} \leq \underline{T}_w < T_{\max}$, there exists a variation of the thrust T like in the proof of Proposition V.2, which results in better time optimality, hence a contradiction. □

Corolory V.1. The optimal control T^* is a combination of $T_{\max}$, $\overline{T}_w$ and $T_{\min}$.

VI. Two Algorithms for Finding the Optimal Control

Recall that the admissible speed set $\mathcal{W}$ depends on the given path. Once the path is given, it is possible to find a semi-analytical solution of the optimal control using the necessary conditions introduced in the previous section. Although in the sequel it is assumed that the initial and final speed-square Ω_0 and Ω_f are fixed, yet the method proposed in this section can be easily extended to the case with free boundary conditions. Assuming that the given path is feasible, then according to Corollary V.1, $\underline{g}_w$ cannot be part of the optimal thrust profile except for the trivial case $\underline{g}_w = \overline{g}_w$.

If the optimal speed profile Ω^* touches the upper boundary $\overline{g}_w$, then necessarily $\Omega^*(s) = \overline{g}_w(s)$ on some (perhaps trivial) intervals. Let $[s_a, s_b] \subseteq [s_0, s_f]$ be the subinterval on which $\Omega^*(s) = \overline{g}_w(s)$. It is possible that $\Omega^*(s) = \overline{g}_w(s)$ for all $s \in [s_a, s_b]$ only if $\overline{T}_w(s) \in [T_{\min}, T_{\max}]$ for all $s \in [s_a, s_b]$, where $\overline{T}_w(s) = \Gamma \circ \overline{g}_w(s)$, $s \in [s_a, s_b]$, as defined in (52).

Let $\widetilde{W}$ be the smooth part of the graph of $\overline{g}_w$ which could possibly be part of Ω^*, given by

$$\widetilde{W} \stackrel{\triangle}{=} \left\{ (s, \overline{g}_w(s)) | \overline{T}_w(s) \in [T_{\min}(s), T_{\max}(s)],\, s \in [s_0, s_f] \right\},$$

and let $\widetilde{W}_d$ be the points of the graph of $\overline{g}_w$ where $\overline{g}'_w$ is discontinuous, which is given by

$$\widetilde{W}_d \stackrel{\triangle}{=} \left\{ (s_d, \overline{g}_w(s_d)) | \lim_{s \to s_d^+} \overline{g}'_w(s) \neq \lim_{s \to s_d^-} \overline{g}'_w(s),\, s_d \in (s_0, s_f),\, s \in [s_0, s_f] \right\}.$$

Let $\overline{W} = \widetilde{W} \bigcup \widetilde{W}_d$. Generally, $\overline{W}$ is disconnected. Depending on the path, $\overline{W}$ may consist of multiple segments of curves and single points, as shown in Fig. 4 (blue curves and points). By the piece-wise analyticity assumption of the given path and the construction of $\overline{g}_w$, there exists a finite index set $\mathcal{J}$ such that $\overline{W} = \bigcup_{j \in \mathcal{J}} \overline{W}_j$, with $\overline{W}_j$ connected for each j, and $\overline{W}_i \bigcap \overline{W}_j$ empty for any $i \neq j$, $i, j \in \mathcal{J}$. Without loss of generality, let $\mathcal{J} = \{1, 2, \ldots, N-1\}$. Let (s_j^-, Ω_j^-) and (s_j^+, Ω_j^+) denote the left and right end points of $\overline{W}_j$ for each $j \in \mathcal{J}$, where $\Omega_j^- = \overline{g}_w(s_j^-)$ and $\Omega_j^+ = \overline{g}_w(s_j^+)$ correspond to the "trajectory sink" and "trajectory source" in Ref. [7]. Also, define two points $\overline{W}_0 = (s_0, \Omega_0)$ and $\overline{W}_{J_f} = (s_f, \Omega_f)$. It's obvious that as required initial and final conditions, $\overline{W}_0$ and $\overline{W}_{J_f}$ must be part of the optimal speed profile.

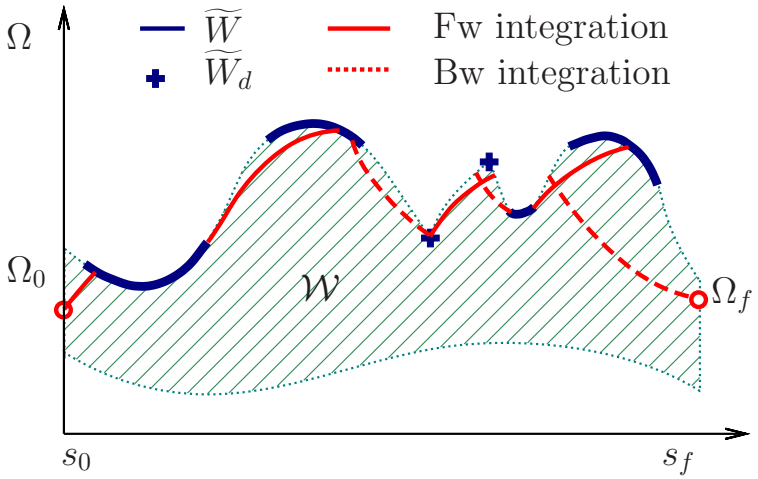

Figure 4. Building elements for the optimal Ω

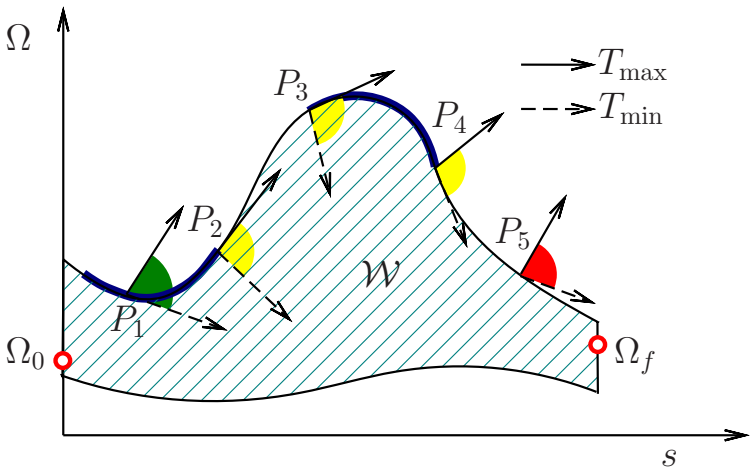

Figure 5. Steering the velocity at the boundary of $\mathcal{W}$

Since the control input $T(s)$ determines the derivative of the speed profile $\Omega(s)$ at s, finding the optimal speed profile can also be understood as steering the point $(s, \Omega(s))$ within $\mathcal{W}$ using the input T in such a way so as to maximize $\Omega(s)$ pointwise. According to Proposition V.2, when the point $(s, \Omega(s))$ in the interior of $\mathcal{W}$, either $T_{\max}$ or $T_{\min}$ should be applied. When $(s, \Omega(s))$ lies on the boundary of $\mathcal{W}$, as shown in Fig. 5, it is required that the thrust either steers the trajectory into the interior of $\mathcal{W}$, or keeps the trajectory on the boundary of $\mathcal{W}$. In Fig. 5, the possible directions of steering on the upper boundary of $\mathcal{W}$ is given by $\Gamma \circ \overline{g}_w(s) \in [T_{\min}, T_{\max}]$, as shown by the shaded area between the arrows. At point P_1, the interior of the green shadow area overlaps $\mathcal{W}$, suggesting that P_1 could be part of the optimal trajectory. At P_2, P_3 and P_4, the purple shaded area overlaps $\mathcal{W}$ only at its boundary, so either $T_{\max}$ or $T_{\min}$ can be applied to steer $(s, \Omega(s))$ within $\mathcal{W}$. At P_5, there is no overlap between the red shaded area and $\mathcal{W}$, so $(s, \Omega(s))$ will move outside $\mathcal{W}$ anyway, which means the optimal speed profile never passes through the point P_5.

According to Theorem V.1, the optimal speed profile consists of a combination of forward integration with input $T_{\max}$, backward integration with $T_{\min}$, and the thrust profile determined by $\overline{W}_j$. Since the set $\mathcal{J}$ is finite, the optimal control can be found from combinations of $\overline{W}_j$ together with $T_{\max}$ and $T_{\min}$ connecting different $\overline{W}_j$.

For each $j = 1, \ldots, N-1$, let $\mathcal{S}_j^+$ denote the forward integration trajectory starting from s_j^+ with the initial value $\mathcal{S}_j^+(s_j^+) \triangleq \Omega_j^+$, which is given by

$$\mathcal{S}_j^+(s) = \Omega_j^+ + \int_{s_j^+}^{s} \left(\frac{T_{\max}}{m} + c_1(\tau)\mathcal{S}_j^+(\tau) + c_2(\tau)\frac{1}{\mathcal{S}_j^+(\tau)} + c_3(\tau) \right) \mathrm{d}\tau,$$

and similarly define $\mathcal{S}_j^-$ to be the backward integration trajectory starting from s_j^- with the initial value $\mathcal{S}_j^-(s_j^-) \triangleq \Omega_j^-$ and control input $T_{\min}$. Forward integration with $T_{\max}$ and backward integration with $T_{\min}$ are also computed from s_0 and s_f with initial conditions Ω_0 and Ω_f respectively, and the resulting trajectories are denoted with $\mathcal{S}_0^+$ and $\mathcal{S}_N^-$. As stated before, the optimal speed profile, if it exists, includes a combination of parts of integration trajectories and $\overline{W}_j$, and is point-wise maximized.

All current algorithms, like those in Refs. [5–8] repeat the "search, integrate and check" process, and gradually extend an optimal speed profile from the initial point to the final point. It is possible that during the search process, part of the previously constructed trajectory is discarded because it cannot pass though the next intermediate control points/curve or points where $\overline{g}_w$ is not analytic, which reduces the efficiency of these algorithms. Next, we introduce two new algorithms which improve the numerical efficiency of the search process for the optimal speed profile. The first algorithm is designed for parallel computation, and the second algorithm reduces the computation spent on the "search, integrate and check" process.

VI.A. Algorithm I

Step 1 Compute $\overline{g}_w$ and $\underline{g}_w$.

Step 2 Calculate $\mathcal{S}_0^+$ at s_0 and $\mathcal{S}_j^+$ for $j = 1, 2, \ldots, N-1$, with the integration terminating when $\overline{g}_w(s) = \mathcal{S}_j^+(s)$, or $s = 0$, or $s = s_f$. Also calculate the backward integration profile at s_f and s_j^- for $\mathcal{S}_j^-$ for $j = 1, 2, \ldots, N$, with the integration terminating when $\overline{g}_w(s) = \mathcal{S}_j^-(s)$. Let $\mathcal{S}_j^+(s) = \overline{g}_w(s)$ and $\mathcal{S}_j^-(s) = \overline{g}_w(s)$ for all s outside their domain of integration.

Step 3 Let

$$\Omega(s) \stackrel{\triangle}{=} \min\{S_0^+(s), S_1^+(s), \ldots, S_{N-1}^+(s), S_1^-(s), S_2^-(s), \ldots, S_N^+(s)\}. \tag{53}$$

If $\Omega(0) = \Omega_0$, $\Omega(s_f) = \Omega_f$ and $\Omega(s) \geq \overline{g}_w(s)$ for all $s \in [s_0, s_f]$, then the optimal speed profile $\Omega^* = \Omega$. Otherwise the given path is not feasible.

The optimal thrust profile T^* is given by $T^* = \Gamma \circ \Omega^*$. By construction, the optimal thrust profile T^* satisfies the necessary conditions given by Proposition V.2 and Corollary V.1. The control T^* is indeed optimal because it maximizes point-wise the speed profile, and any further increase in speed results in the violation of the speed constraint.

Note that the "search, integrate and check" process is avoided in this algorithm. This algorithm can be easily implemented in parallel computation owing to the following reasons: (i) Step 1 and Step 3 can be performed point-wise for different $s \in [s_0, s_f]$; (ii) in Step 2 the computations of $\mathcal{S}_j^-$ and $\mathcal{S}_j^+$ are independent, hence they can be computed in different processors for different $j \in \mathcal{J}$ at the same time.

VI.B. Algorithm II

The following algorithm still preserves the "search, integrate and check" process, but the repetition of the process is reduced to a minimum.

Step 1 Compute $\overline{g}_w$ and $\underline{g}_w$.

Step 2 Compute $\mathcal{S}_0^+(s)$ and $\mathcal{S}_N^-(s)$ with stopping criteria $\mathcal{S}_0^+(s) = \overline{g}_w(s)$ and $\mathcal{S}_N^-(s) = \overline{g}_w(s)$, or $s = s_0$, or $s = s_f$. Update $\overline{g}_w(s) = \mathcal{S}_0^+(s)$ and $\overline{g}_w(s) = \mathcal{S}_0^-(s)$ on the corresponding domain of integration. If the graph of $\overline{g}_w$ does not intersect $\overline{W}^c$, or $\overline{g}_w(s_0) \neq \Omega(s_0)$ or $\overline{g}_w(s_f) \neq \Omega(s_f)$, then go to Step 4. Otherwise denote the union of the domain of integration for $\mathcal{S}_0^+(s)$ and $\mathcal{S}_N^-(s)$ with $\mathcal{I}$ and go to the next step.

Step 3 Among those $\overline{W}_j$ which are below the graph of $\overline{g}_w$, select the one which is closest to the s axis. Let its index be k. If no $\overline{W}_j$ is below the graph of $\overline{g}_w$, then go to Step 4, otherwise compute $\mathcal{S}_k^-(s)$ and $\mathcal{S}_k^+(s)$ with the stopping criteria $\mathcal{S}_k^-(s) = \overline{g}_w(s)$ and $\mathcal{S}_k^+(s) = \overline{g}_w(s)$, , or $s = 0$, or $s = s_f$. Update $\overline{g}_w(s) = \mathcal{S}_k^-(s)$ and $\overline{g}_w(s) = \mathcal{S}_k^+(s)$ on the corresponding domain of integration. If the graph of $\overline{g}_w$ does not intersect $\overline{W}^c$, or $\overline{g}_w(s_0) \neq \Omega(s_0)$ or $\overline{g}_w(s_f) \neq \Omega(s_f)$, otherwise repeat the same step.

Step 4 If $\overline{g}_w$ does not pass through the initial and final points, then the given path is infeasible. Otherwise, the optimal speed profile is given by $\Omega^* = \overline{g}_w$.

The difference between Algorithm II and the other time-optimal control algorithms in Refs. [5–8] is illustrated in Fig. 6. While Algorithm II computes only the integrations which are involved in the construction of the optimal speed profile, the other algorithms integrate the trajectory along arcs which may latter be discarded when extending the optimal speed profile to the final point, hence are less efficient compared to Algorithm II.

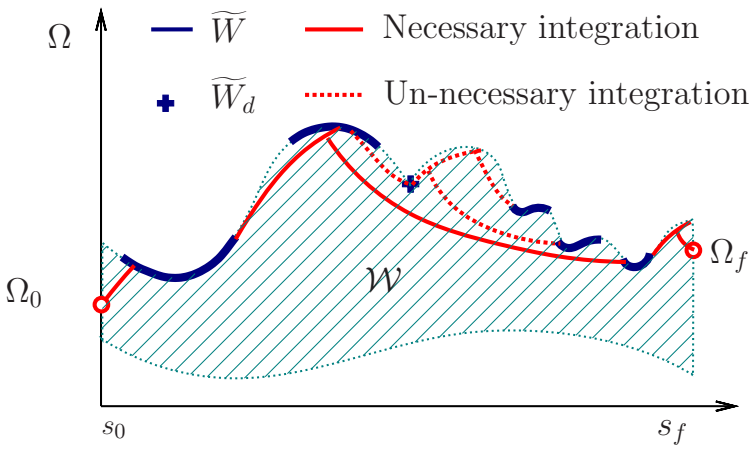

Figure 6. Algorithm comparison

VII. Numerical Examples

In this section, two examples are used to test the feasibility and optimality of the proposed optimal time parameterization method. Both examples implement Algorithm II. The first example examines whether the controls given by the optimal parameterization method satisfy the prescribed bounds, and whether the aircraft can follow the path when using these control inputs. In the second example, the given path is a minimum-time path with known time parameterization, and is used to examine the optimality of the proposed method.

VII.A. Aircraft with Constant Rate Turning

A three-dimensional path is used to test the proposed time parameterization method. The trajectory is shown in Fig. 7. The initial position of the aircraft is $(0, 0, 6)$ km, the aircraft flies at v_0=120 m/s (268.4 mph), 0° path angle and 0° heading. The final position is (111.0,17.3,0) km, with final speed v_f=85 m/s (212.5 mph), 0° path angle and -25° heading. The horizontal projection of the trajectory contains two constant rate turning maneuvers. The vertical velocity profile contains three phases: the aircraft first going downward with constant vertical acceleration -0.1 g, then descending at a constant vertical speed, and finally decelerating to zero with constant vertical acceleration 0.1 g until it arrives at the final position. The atmospheric density data are taken from Ref. [15]. The change of gravity with altitude is neglected.

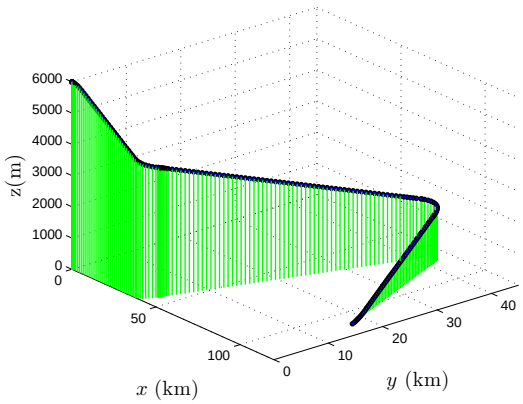

Figure 7. 3D Geometric Trajectory.

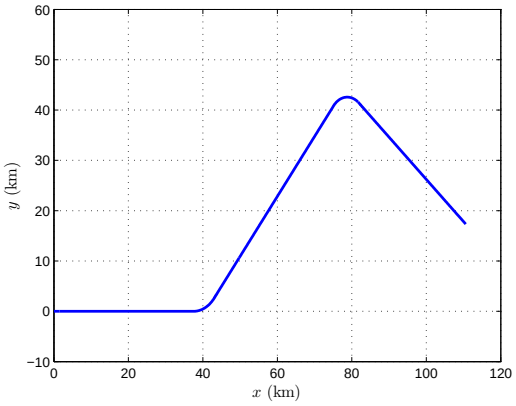

Figure 8. X-Y plane projection of the geometric trajectory.

The control bounds are given as follows: the lift coefficient $C_L \in [0.067, 1.9]$, the bank angle $\phi \in [-20^\circ, 20^\circ]$, and the thrust $T \in [0, 137.8]$ kN. It is also required that the speed does not violate the up-

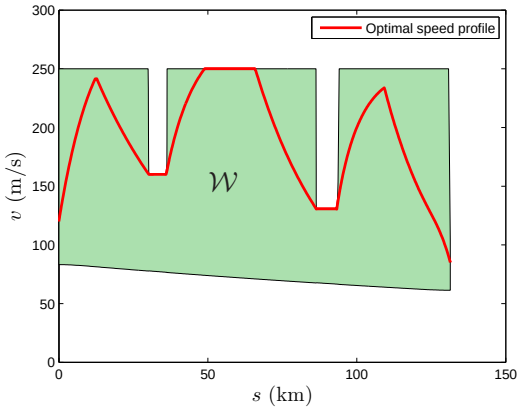

Figure 9. Optimal speed profile under path coordinate.

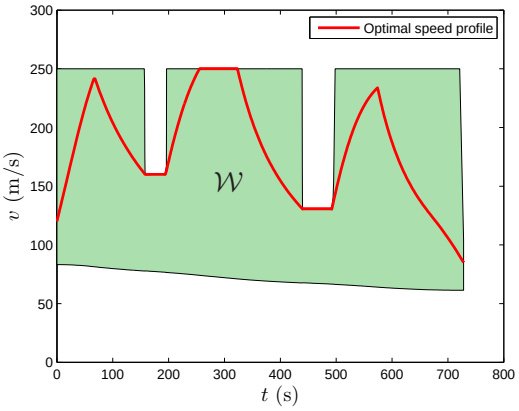

Figure 10. Time history of optimal speed.

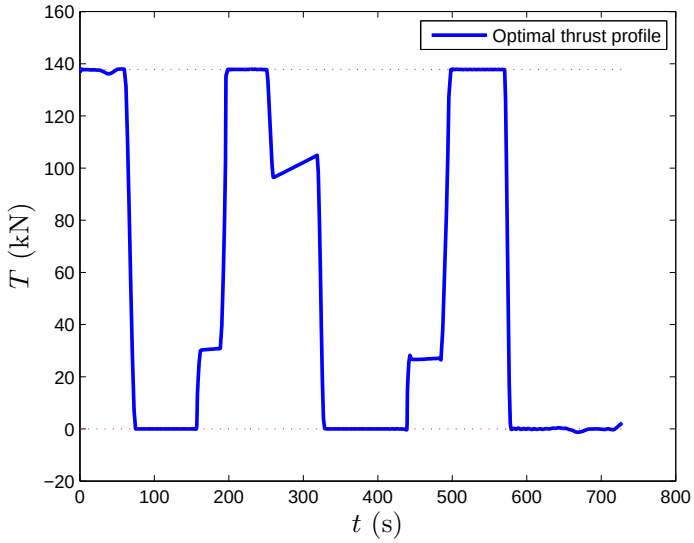

Figure 11. Optimal thrust.

per limit of $v_{\max}$=250 m/s (559.2 mph) or the lower limit $v_{\min}$=60 m/s (134.2 mph). Using the optimal time parameterization method, the minimum-time speed profile $v^*(s)$ is computed using parameters similar to those of a large commercial aircraft. The optimal speed profile along the path is shown in Fig. 9. The same profile in terms of time is shown in Fig. 10. To arrive at the final position in minimum time, the aircraft should fly as fast as possible, however, due to the limited acceleration and deceleration capability, the optimal velocity profile cannot necessarily stay at $v_{\max}$ all the time. As can be seen from Fig. 9, the left turning maneuver results in a maximum speed limit of 160 m/s, while the second right turning results in a speed limit of 130.5 m/s. Within $0 \leq s \leq 30$km, the upper limit of speed is 250 m/s, but the aircraft cannot travel at the maximum speed because it would not be able to decelerate sufficiently, and would violate the speed upper limit within 30km $\leq$ s $\leq$ 36km, which is induced by the first left turning maneuver. Similar scenarios exist before the second turning maneuver and the final point. The total length of the path is 131.4 km, and the aircraft finishes in 728 s using the optimal thrust with an average speed of 180.5 m/s.

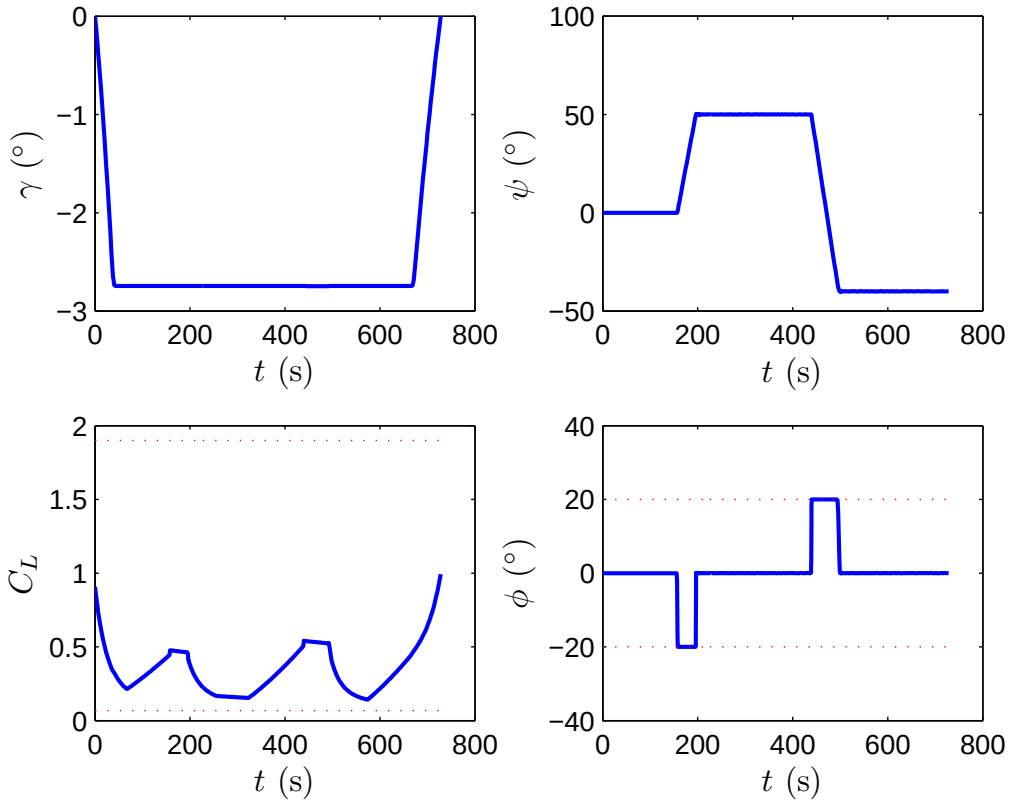

Figure 12. The states and control histories of the time parameterized trajectory.

The state and control histories recovered from the optimally time-parameterized trajectory are shown in Fig.12. The red dotted lines in the figures represent the control bounds. As shown in the figure, the thrust and bank angle saturate during some phases of the flight. The saturations of the bank angle are caused by the turning maneuvers. The saturation of the thrust leads to maximum acceleration which improves optimality.

To check the validity of the time parameterization result, inverse dynamics are used to recover the state and control histories from the optimal time parameterization result $\big(x^*(t), y^*(t), z^*(t)\big)$. Ideally, flying the optimally time-parameterized path should not result in any violation of the control constraints.

For the purpose of validation, after the control histories are calculated from inverse dynamics, they are used as the control inputs to simulate the trajectory. Specifically, the ordinary differential equations (1)-(6) are solved using the resulted control histories. The new simulated trajectory $(\hat{x}, \hat{y}, \hat{z})$ is compared with (x^*, y^*, z^*) in Fig. 13.

The discrepancy between the simulated trajectory and the original input trajectory is estimated using

the following relative error index

$$\Delta_r = \max_t \sqrt{\left(\frac{\hat{x}(t) - x^*(t)}{\max_t x^*(t) - \min_t x^*(t)}\right)^2 + \left(\frac{\hat{y}(t) - y^*(t)}{\max_t y^*(t) - \min_t y^*(t)}\right)^2 + \left(\frac{\hat{z}(t) - z^*(t)}{\max_t z^*(t) - \min_t z^*(t)}\right)^2}$$

For this example, $\Delta_r = 8.9e-3$, which is quite acceptable

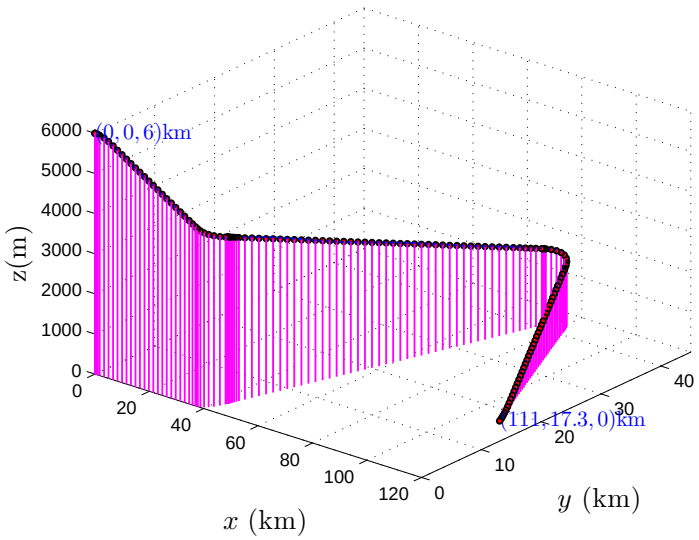

Figure 13. Comparison of the original geometric path(dots) and the path generated using time parameterization and inverse dynamics(line).

VII.B. Time Optimal Path

In order to validate the time optimality of the time-parameterized trajectory, a minimum-time landing trajectory for a large civil aircraft is used to test the proposed method. The trajectory is generated using the DENMRA, which solves optimal control problems with an automatic multiresolution mesh refinement scheme.[16,17] The accuracy and robustness of the DENMRA have been illustrated in the same references. The aircraft starts at an initial position of $(0, 0, 10)$km, and lands at an airport with position (110,-60,0) km. The initial conditions are: speed $v(0)$=240 m/s (537 mph), heading angle $\psi(0) = 0^\circ$ and the path angle $\gamma(0) = 0^\circ$; the final conditions are: speed $v(s_f)$=95 m/s (212.5 mph), heading angle $\psi(s_f) = 80^\circ$, and path angle $\gamma(s_f) = -3^\circ$. The aircraft considered in this example is DC-9-30. During the whole flight, the following constraints need to be satisfied: $v \leq 260$ m/s (581.6 mph), $\phi \in [-15, 15]^\circ$, $C_L \in [-0.31, 1.52]$, and $T \in [0, 137.8]$ kN. The path is shown in Figs. 14 and 15.

Because this is a minimum-time path, the time parameterization given by DENMRA is optimal. Therefore, when applying the parameterization method in this paper to the path given by DENMRA, the optimal time parameterization result is expected to agree with the DENMRA result.

The optimal parameterization method gives a total travel time of 581.39 s, which matches very well with the final time of 581.36 s given by the DENMRA. The admissible speed set $\mathcal{W}$ in terms of the path coordinate and time are shown in Figs. 16 and 17, respectively. The time history of the speed and the controls are shown in Figs. 18-21. As mentioned before, the other two states—the path angle γ and the heading angle ψ—are pure geometric variables, and are independent of parameterization, so they are not used for checking the optimality of the proposed method. It should be noted that since the DENMRA uses a smoothness enhancement technique for this optimal landing problem to guarantee the convergence of the solution, it can be seen from these figures that the results are slightly smoother than those given by the optimal parameterization method.

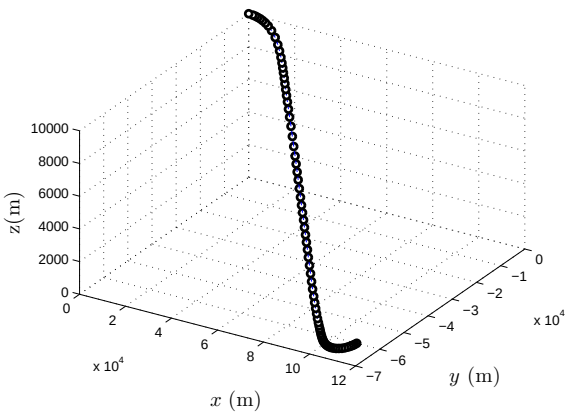

Figure 14. the min-time trajectory.

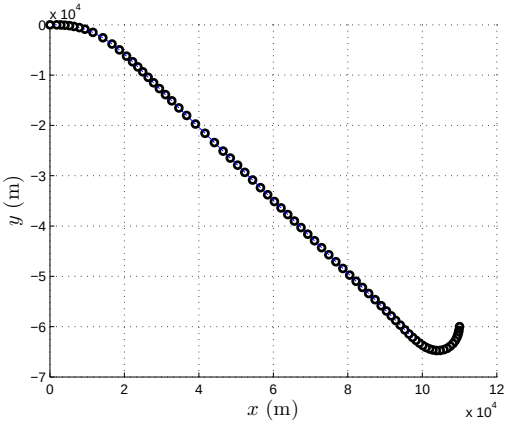

Figure 15. X-Y plane projection of the min-time trajectory.

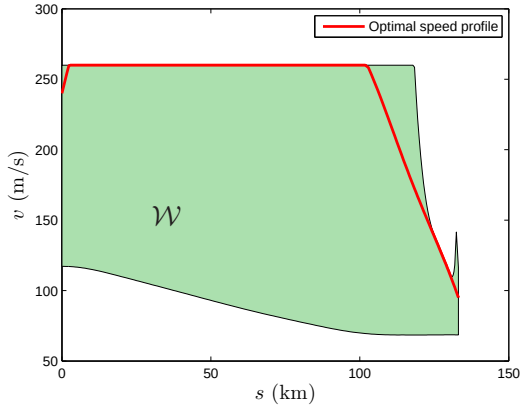

Figure 16. Optimal speed profile under path coordinate (DENMRA).

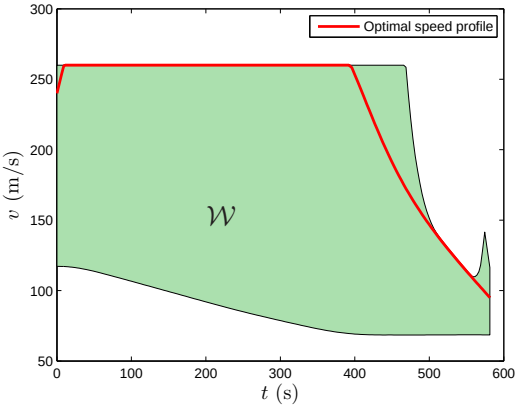

Figure 17. Time history of optimal speed (DENMRA).

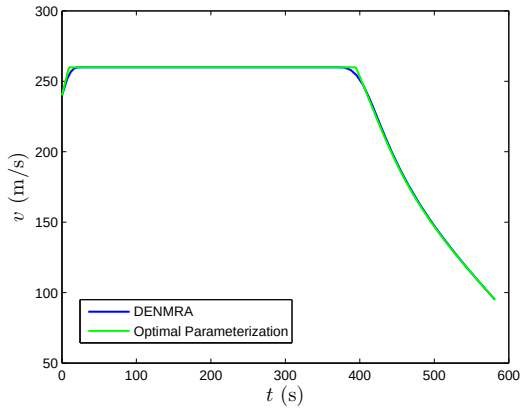

Figure 18. Speed comparison.

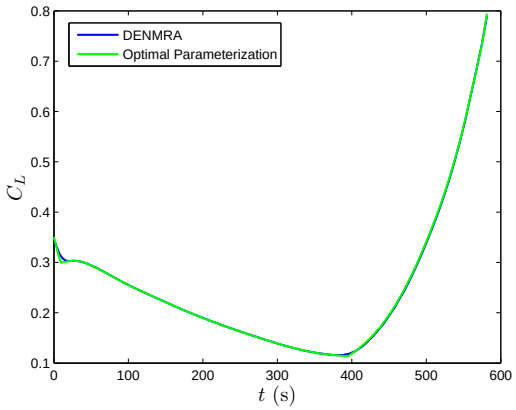

Figure 19. Control comparison: C_L.

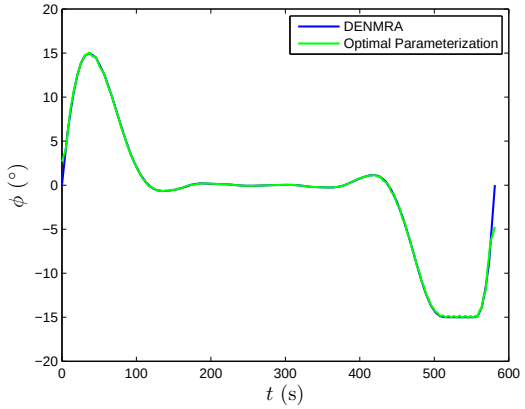

Figure 20. Control comparison: ϕ.

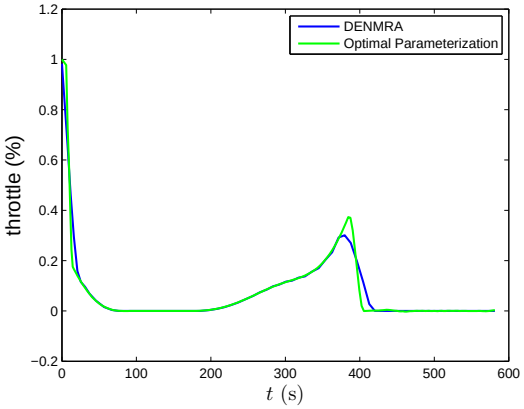

Figure 21. Control comparison: throttle.

VIII. Conclusions

The problem of minimum-time-travel for a fixed-wing aircraft along a specified path has been addressed. The time-optimal control problem was studied with an emphasis on the effects of differential and algebraic constraints involving the controls. The use of intermediate control in the time-optimal control of second order systems like aircraft or robotic manipulators are the result of active algebraic constraints on speed, which may either be specified a priori, or come from degenerated differential constraints that manifest themselves as algebraic constraints. In an interval where the speed constraint is not active, there exists at most one switch which is from the maximum thrust to the minimum thrust, hence the switching structure (of bang-bang control) for the time-optimal control problem is unique. The admissible speed set is introduced to characterize the domain within which the optimal speed profile is searched. The admissible speed set is generated by considering both the algebraic constraints and the differential constraints, hence a search within the admissible speed set naturally addresses the intermediate control problem. Two algorithms are proposed, based on the unique control switching structure and the admissible speed set. The first algorithm can be easily implemented in parallel, which is difficult for other algorithms involving a sequential "search, integrate and check" pattern. The second algorithm improves the numerical efficiency by eliminating unnecessary integrations.

It has been verified through numerical examples that the optimally time-parameterized trajectory satisfies the specified control bounds, and is indeed flyable with control histories which can be obtained from the time-parameterized solution. The time parameterization method, when combined with other fast time geometric path planning methods[18] leads to feasible trajectories as opposed to just feasible paths. Furthermore, the proposed Algorithms I and II improve computation time by eliminating or reducing the "search, integrate and check" pattern, and are suitable for real-time implementations.

Acknowledgment: This work has been supported by NASA with contract no. NNX08AB94A, by NASA Ames Research Center. Contract monitor is Corey Ippolito.

References

[1]Nilsson, N. J., *Principles of Artificial Intelligence*, Tioga Publishing Company, Palo Alto, CA, 1980.

[2]Stentz, A., "Optimal and Efficient Path Planning for Partially-Known Environments," *IEEE International Conference on Robotics and Automation*, 1994.

[3]Dubins, L. E., "On Curves of Minimal Length with a Constraint on Average Curvature, and with Prescribed Initial and Terminal Positions and Tangents," *American Journal of Mathematics*, Vol. 79, No. 3, 1957, pp. 497–516.

[4]Chuang, J. and Ahuja, N., "Path Planning using Newtonian Potential," *IEEE Conference on Robotics and Automation*, Sacramento, CA, 1991, pp. 558–563.

[5]Bobrow, J. E., Dubowsky, S., and Gibson, J. S., "Time-Optimal Control of Robotic Manipulators Along Specified Paths," *The International Journal of Robotics Research*, Vol. 4, No. 3, 1985, pp. 3–17.

[6]Shin, K. G. and McKay, N. D., "Minimum-Time Control of Robotic Manipulators with Geometric Path Constraints," *IEEE Transactions on Automatic Control*, Vol. AC-30, No. 6, June 1985, pp. 531–541.

[7]Pfeiffer, F. and Johanni, R., "A Concept for Manipulator Trajectory Planning," *IEEE Journal of Robotics and Automation*, Vol. RA-3, No. 2, April 1987, pp. 115–123.

[8]Shiller, Z. and Lu, H.-H., "Computation of path constrained time optimal motions with dynamic singularities," *Journal of Dynamic Systems, Measurement, and Control*, Vol. 114, No. 1, Mar 1992, pp. 34–40.

[9]Shiller, Z., "On Singular Time-Optimal Control Along Specified Paths," *IEEE Transactions on Robotics and Automation*, Vol. 10, No. 4, August 1994, pp. 561–566.

[10]Miele, A., "Optimal trajectories and guidance trajectories for aircraft flight through windshears," *Proceedings of the 29th IEEE Conference on Decision and Control*, Vol. 2, Honolulu, HI, Dec 1990, pp. 737–746.

[11]Carlson, E. B. and Zhao, Y., "Optimal Short Takeoff of Tiltrotor Aircraft in One Engine Failure," *Journal of Aircraft*, Vol. 39, No. 2, Mar-Apr 2002, pp. 280–289.

[12]Ross, I. M. and Fahroo, F., *New Trends in Nonlinear Dynamics and Control and their Applications*, Vol. 295, chap. Legendre Pseudospectral Approximations of Optimal Control Problems, Springer Berlin / Heidelberg, 2004, pp. 327–342.

[13]Jain, S. and Tsiotras, P., "Trajectory Optimization Using Multiresolution Techniques," *Journal of Guidance, Control, and Dynamics*, Vol. 31, No. 5, 2008, pp. 1424–1436.

[14]Etkin, B., *Dynamics of Atmospheric Flight*, Dover Publications, 2005.

[15]NASA, "Earth atmosphere model," http://www.grc.nasa.gov/WWW/K-12/ airplane/ atmosmet.html, retrieved Aug, 2009.

[16]Zhao, Y. and Tsiotras, P., "A Density-Function Based Mesh Refinement Algorithm for Solving Optimal Control Problems," *Infotech at Aerospace Conference, Seattle, WA*, 2009, AIAA-2009-2019.

[17]Zhao, Y. and Tsiotras, P., "Mesh Refinement for Solving Optimal Control Problems Using Grid Density Functions," *Journal of Guidance, Control and Dynamics*, submitted.

[18]Bakolas, E. and Tsiotras, P., "Multiresolution Path Planning Via Sector Decompositions Compatible to On-Board Sensor Data," *AIAA Guidance, Navigation and Control Conference and Exhibit*, Honolulu, Hawaii, Aug. 2008.